Article

Green Organo-Photooxidative Method for the Degradation of Methylene Blue Dye

Adnan Majeed, Ahmad H. Ibrahim, Sawsan S. Al-Rawi, Muhammad Adnan Iqbal,* Muhammad Kashif, Muhammad Yousif, Zain Ul Abidin, Shahzaib Ali, Muhammad Arbaz, and Syed Arslan Hussain
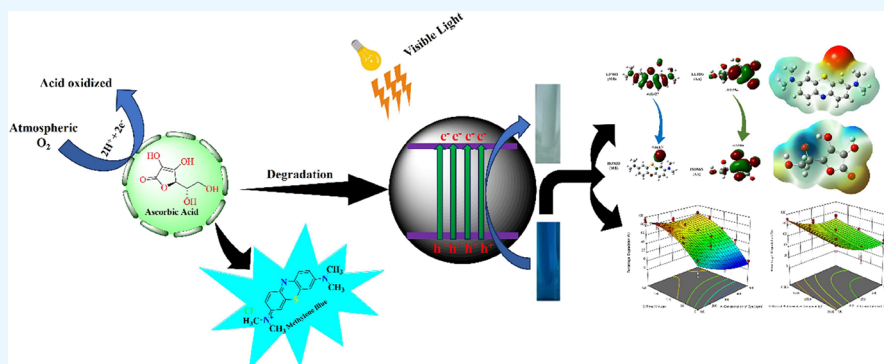
Read Online

ACCESS | Metrics & More | Article Recommendations | Supporting Information

ABSTRACT: This study used an organophoto-oxidative material to degrade the toxic azo dye, methylene blue (MB), due to its hazardous effects on aquatic life and humans. MB is traditionally degraded using metal-based catalysts, resulting in high costs. Several organic acids were screened for organo-photooxidative applications against various azo dyes, and ascorbic acid (AA), also known as vitamin C, was found to be best for degradation due to its high photooxidative activity. It is an eco-friendly, edible, and efficient photooxidative material. A photocatalytic box has been developed for the study of organo-photooxidative activity. It was found that when AA was added, degradation efficiency increased from 42 to 95% within 240 min. Different characterization techniques, such as HPLC and GC-MS, were used after degradation for the structural elucidation of degraded products. DFT study was done for the investigation of the mechanistic study behind the degradation process. A statistical tool, RSM, was used for the optimization of parameters (concentration of dye, catalyst, and time). This study develops sustainable and effective solutions for wastewater treatment.

1. INTRODUCTION

During the past few years, environmental concerns have gained more attention. The public, particularly entrepreneurs, are concerned about conditions that negatively impact the environment,[1,2] such as industrialization and urbanization that have affected the quality of water supplies.[3] Chemical contamination, especially wastewater generated by the textile industries, contains a significant amount of colors and toxic synthetic mixtures that are responsible for environmental toxicity[4] and have affected the clarity and taste of water, making it unpleasant to consumers.[2,5] Water is one of the most valued assets on earth, but it contains a lot of pollutants, including metal ions,[6] anions,[7] phenol,[8] dyes,[9] detergents,[10] and pesticides.[11] Textile dyeing uses a dye pigment to color the products, and the dye causes problems with light penetration into water and interference with photosynthesis as well as with human beings.[11,12] In addition to being toxic and carcinogenic, some dyes pose a serious environmental and human health risk.[13] Methylene blue (MB) is a heterocyclic aromatic

compound mostly used for dyeing silk, cotton, and also for indication of chemical change.[14] Its presence in wastewater is extremely hazardous. A variety of medical[15] and biological[16] applications use MB. Due to its water solubility, MB causes pollution in aquatic, human, and animal food chains when discharged directly into the water without prior treatment.[17] There are several health risks associated with the release of partially or untreated wastewater containing MB dye from any of the aforementioned industries.[18] A high intake of MB may lead to several serious health problems, including shortness of breath, burning sensations, chest pain, cancer, cyanosis, tissue necrosis, Heinz body formation, vomiting, jaundice, shock,

enhanced heartbeat rate, and painful micturition.[18,19] Furthermore, MB has become a major problem for plants, such as inhibiting growth and reducing pigment.[20] For these reasons, MB was chosen as the model dye for degradation. Thus, efficient methods are required to remove dye contaminants from effluents to protect water reservoirs.[21]

The treatment of dye wastewater involves physical methods such as reverse osmosis,[22] electrodialysis,[23] nanofiltration,[24] and various chemical methods like coagulation,[25] redox reactions,[26] adsorption[27] ozonation,[28] microbial degradation,[29] and photocatalysis.[12] The strong aromatic and structural properties of these dyes make them difficult to degrade. Among these techniques, photooxidative degradation stands out as a cost-effective, sustainable, eco-friendly, and easy process that occurs on the catalyst surface.[30]

Over the past several years, photochemistry has undergone a renaissance.[31] In addition, metal-based photocatalysts were involved in studies of Sharma et al.[32] where magnetic spinel ferrites MFe_2O_4 (M = Cu, Zn, Ni, and Co) were used in the photo-Fenton process which described the degradation of MB; the addition of H_2O_2 showed that $CuFe_2O_4$ has high reactivity as compared to others such as $ZnFe_2O_4$, $NiFe_2O_4$, $CoFe_2O_4$,[33] TiO_2, ZnO, and plasmonic metals (like Ag, Au, and pt) which were also successfully employed for efficient degradation but their potential for photoredox catalysis to create novel reactivity is limited by conventional polar reactions.[34] Many efficient catalysts have been introduced by researchers in the past, but organo-photooxidative materials have been recently explored because of their oxidative properties and stability. They are usually nontoxic, inexpensive, robust, and inert toward conditions like moisture and oxygen.[35] Organo-photooxidative material may be called organo-catalysts during the use of small organic molecules to facilitate diverse asymmetric transformations, providing a versatile approach to compound synthesis in the presence of light.[36] Among asymmetric catalysis, biocatalysis, and transition metal catalysis, it has gained fundamental importance and attracted the attention of scientists because of its unique and interesting properties.[37] The 2021 Nobel prize in chemistry was presented for a groundbreaking chemical discovery: "the development of asymmetric organo-catalysis".[38] In the past, degradation of MB was carried out by various catalysts, but the most effective and green method to degrade the dye may be organo-photo-oxidative. Organic molecules as oxidative materials, without the involvement of inorganic elements, have emerged as a rapidly growing field of chemical research. The application of the organo-photooxidative method to dye degradation reduces the environmental impact of synthetic dyes by improving efficiency and sustainability.[39] This method is more attractive than other methods due to the lower cost of catalysts and the use of renewable energy.[40] There are various organo-photooxidative materials for the degradation of azo dyes, such as tartaric acid, oxalic acid, acetic acid, maleic acid, and ascorbic acid (AA). Based on their photooxidative activity in this work, L-ascorbic acid (AA) is used as a photooxidative substance after screening several organic compounds for the dye degradation of MB and can provide complete elimination of pollutants from the environment; their chemical structures are shown in Figure S1 (Supporting Information) due to the higher degradation efficiency of this photooxidative substance. The water-soluble organic photooxidative AA, also known as vitamin C, can be an eco-friendly and hydrogen-bonding

material that has been used for a wide range of chemical transformations over the years.[41]

Due to its versatility, availability, and ease of handling, it is a highly appealing photooxidative compound.[42] The main purpose of this work was to examine the degradation ability of AA to obtain a higher photooxidative degradation rate for the removal of MB dye from wastewater. To calculate the degradation time of azo dye under numerous conditions and to analyze the concentration influences of acid and azo dye during the organo-photooxidation reaction, a wide range of factors, including various dye concentrations, photooxidative compound dosages, and contact times, were used in the experimental investigations to fully evaluate their impact on color removal effectiveness and degradation performance. There are many approaches to evaluate the organo-photo-oxidation process which are dependent on the change of one variable, such as dye concentration, photooxidative compound dose, and time variation while keeping all other variables constant. As the traditional methods are costly and time-consuming, alternative statistical analysis RSM has been utilized for the optimization of experimental design. Its main purpose is to establish relationships between independent variables and responses.

2. RESULTS AND DISCUSSION

2.1. Spectrophotometric Analysis. Degradation of MB using AA as an organo-photooxidative material has been examined under UV−visible light irradiations at the maximum wavelength (λ_{max}) 664 nm,[43] and absorption spectra of pure and degraded samples of MB is shown in Figure 1. Before
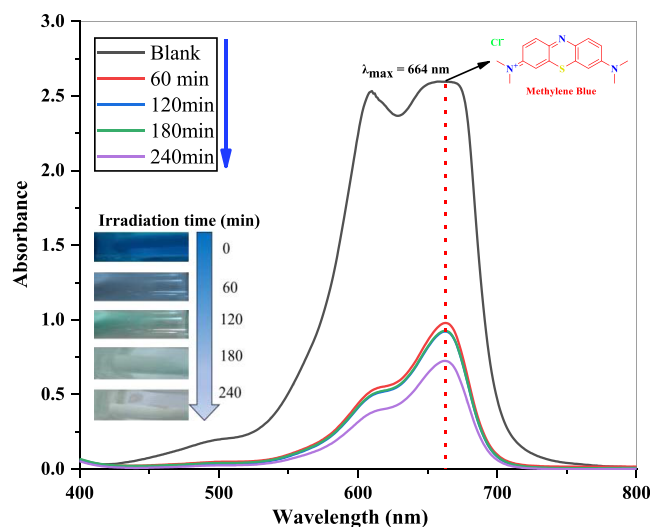

Figure 1. UV−visible absorbance spectra of pure MB alongside degraded MB samples occurred at various time durations, ranging from 0 to 240 min with intervals of 1 h in the presence of AA.

starting the experimental measurements, the radiation source (100W tungsten bulb) was illuminated for some time to maintain the temperature inside the photocatalytic box and the photooxidative material and dye solution were kept 15 cm from the light source.[44] In the presence of a photooxidative material, MB degraded slightly, which indicates that the reaction is oxidation-assisted. After the time intervals of 60, 120, 180, and 240, the value of absorbance was calculated to indicate that MB was degraded gradually with time in the

Table 1. Results of the ANOVA Study of the Quadratic Models for % Degradation of MB

source	sum of squares	df	mean square	F-value	p-value	
model	1.206×10^{05}	9	13404.73	99.75	<0.0001	significant
A − concentration of dye	14591.13	1	14591.13	108.58	<0.0001	
B − dose of photooxidative compound	6178.37	1	6178.37	45.98	<0.0001	
C − time	84690.28	1	84690.28	630.23	<0.0001	
AB	137.77	1	137.77	1.03	0.3132	
AC	2630.76	1	2630.76	19.58	<0.0001	
BC	0.5735	1	0.5735	0.0043	0.9480	
A^2	2803.40	1	2803.40	20.86	<0.0001	
B^2	21.75	1	21.75	0.1618	0.6882	
C^2	9588.50	1	9588.50	71.35	<0.0001	
residual	16797.51	125	134.38			
cor total	1.374×10^{05}	134				

presence of oxidative materials. The peak intensity decreases with time, and the color of the dye also changes from time to time. At the end of 240 min, the peak intensity was close to zero and the characteristic color of the MB was due to the presence of chromophore resulting in the breakdown of the azo bond, indicating that dyes were degraded with time. The results showed 95% of MB photooxidative degradation using AA as an organo-photooxidative material.

2.2. Statistical Analysis. *2.2.1. RSM-Based Optimization of Variables.* The experimental design with experimental values of the MB process was performed as shown in Table S1 (Supporting Information). To fit the experimental data, second order polynomial model is used.[45] It was determined by the design expert that 135 sets of experiments (including with and without addition of photooxidative agent) had their corresponding response (% degradation). In Tables S1 and S2 (Supporting Information), the three independent variables are listed along with their corresponding responses (% degradation) and absorbance of blank MB. A model *F*-value of 99.75 indicates that the model is significant. The probability of a large *F*-value arising from noise is only 0.01%. The significant model terms are A, B, C, AC, A2, and C2. Model terms with values greater than 0.1 are not significant.

Table S1 (Supporting Information) shows the central composite design (CCD) matrix of MB percentage degradation. MB percentage degradation is studied using quadratic models in Table 1. Each coefficient was tested for significance using the *F* test and *p*-value. For the model terms to be significant, Prob > *F* must be less than 0.05 and greater than 0.1000.[46] The value of R^2 was 0.88, while the predicted R^2 and adjusted R^2 were 0.85 and 0.87, respectively, which implies a difference of less than 0.2. A comparison between the coefficient of determination R^2 and adjusted R^2 is used to estimate the model using AA; there was a stronger correlation between the factors and predicted degradation of MB.

It is generally necessary to have a signal-to-noise ratio greater than 4 to calculate an acceptable level of precision. In this study, the degradation percentage of MB was measured with a precision of 36.18. If the ratio exceeds 4, then, the representative may be used to navigate the design space.[47]

A comparison of the experimental and projected degradation values of MB with those of AA is shown in Figure 2. According to the results, there is a large difference between the experimental and predicted values for dye degradation, and the current model is well-suited to fit the experimental results. Accordingly, the model allows for the calculation of dye degradation in the range of variables investigated.
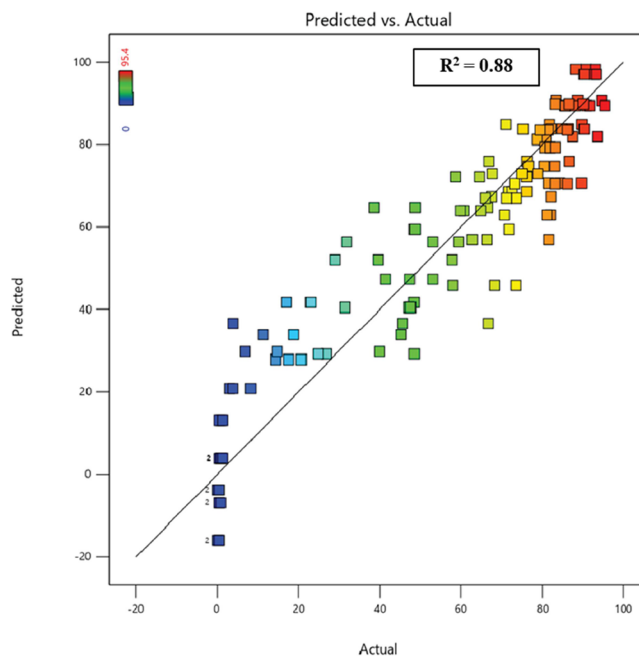

Figure 2. Plot of the predicted versus actual % degradation efficiency.

The plot of residuals against the normal probability for MB degradation is shown in Figure 3. In the plot, the resulting data indicate a linear relationship, which shows an analysis of the residual's distribution. Consequently, the quadratic model developed to parametrize the degradation of MB accurately predicts the experimental results. Figure 4 also verifies that the model has good predictability and requires no transformation of model responses.

2.2.2. Estimation Method Based on Response Surface Plotting. *2.2.2.1. Influence of Dye Concentration.* As a function of time and catalyst dose, Figure 5a shows the effect of dye concentration at the initial stage on photodegradation efficiency. When the dye concentration is low and the dose of the photooxidative substance is increased from 0.004 to 0.006 g, degradation efficiency increases from 79 to 88% at a contact time of 120 min, and by increasing dye concentration to 500 ppm, it decreases from 88 to 41%. Higher dye concentrations may result in a decrease in degradation efficiency because photon paths are shorter in highly colored solutions. This resulted in fewer photons reaching the organic acid's surface.[48]

2.2.2.2. Influence of Catalyst Dose. Figure 5b illustrates the effect of the dosage of the photooxidative substance on
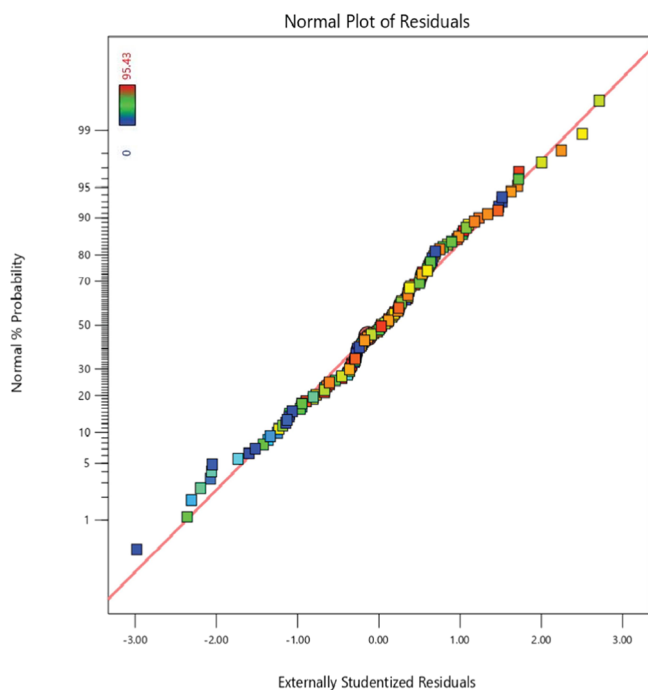
Figure 3. Illustration of the normal probability of raw residuals.
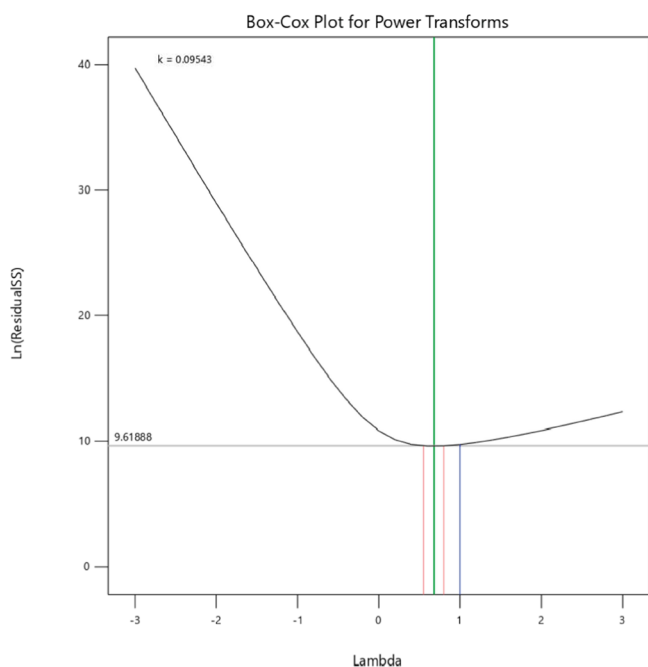

Figure 4. Box−Cox plot of the model.

degradation efficiency when MB concentration is 300 ppm and contact time is 240 min. AA dosage increased from 0.002 to 0.006 g, increasing degradation efficiency from 58 to 86% with an increase in time. The percentage degradation efficiency increased by increasing the active sites by improving the photooxidative substance dosage.[47]

2.2.2.3. Influence of Time. Figure 5c shows the effects of reaction time on MB degradation efficiency at 0.004 g dose and 240 min reaction time. The degradation productivity increases as time increases, but it decreases as the dye concentration increases from 100 to 500 ppm. The results

showed that the degradation efficiency decreased as dye concentration increased.[49]

2.3. FT-IR Analysis. Numerous bands are obtained in FT-IR spectra of MB before and after degradation, as shown in Figure 6 with patterns (a) and (b), respectively. The FT-IR pattern of MB before degradation is shown in Figure 6a. Notable bands can be observed at 3438, 2927, 1586, 1485, 1381, 1313, 1143, 880, and 665 cm^{-1}. The absorption band at 3438 cm^{-1} corresponds to intermolecular hydrogen bonding, involving O−H interactions within adsorbed water molecules from the surrounding environment.[50] The slight absorption band at approximately 2927 cm^{-1} results from the stretching vibration of C−H bonds in methylene.[51] The strong absorption band that appeared at 1586 cm^{-1} corresponds to the stretching vibration of the skeletal structure of the benzene ring.[51] Additionally, absorption bands centered around 1485 and 1381 cm^{-1} indicate stretching vibrations involving C−N bonds in aromatic amines, and this is no longer present in degraded MB.[52] The split band near 1313 cm^{-1} appeared due to the symmetric and asymmetric stretching vibrations of −CH$_3$ groups.[53] An absorption peak around 1143 cm^{-1} signifies the C−N bonds due to stretching vibration within the aliphatic chain.[54] The appearance of a peak at 880 cm^{-1} is attributed to the characteristic absorption resulting from C−H in-plane bending vibrations.[55] Mostly, metal oxides have absorption peaks in the fingerprint region, that is, below 1000 cm^{-1}, due to interatomic vibrations.[56] After the degradation of MB, there were various peak differences observed as shown in Figure 6b. Bands after the degradation of MB are 3527, 3406, 3308, 3209, 3026, 2916, 1753, 1654, 1474, 1319, 1120, and 870 cm^{-1}. A new absorption peak at 3527 cm^{-1} is present and attributed to the stretching of the O−H group in water molecules.[57] A vibrational band at 3406 cm^{-1} in the degraded dye is present instead of pure dye due to -NH/−OH overlapped stretching vibration.[58] The absorption band at 3308 appeared in degraded dye instead of pure dye due to −OH stretching.[59] The absorption bands at 3209 and 3026 cm^{-1} appeared in degraded dye due to stretching and bending vibration of −NH in the amide group.[60,61] The absorption band at 2916 cm^{-1} identified the C−H antisymmetry being the same as 2927 cm^{-1} before degradation, and a decrease in wavenumber from 2927 to 2916 cm^{-1} indicates that the blueshift changes into redshift.[62] The less intense peak disappeared in pure dye but was present in the degraded dye at 1753 cm^{-1} due to heterocyclic aromatic C−N bonds.[60] A new highly intense peak appeared at 1654 cm^{-1} due to the OH bending mode of the adsorbed water molecules on the surface.[63] The increase in wavenumber from 1586 to 1654 cm^{-1} indicates that the redshift changes into a blueshift assigned to C=O.[64] The decrease in wavenumber from 1485 to 1474 cm^{-1} and increase from 1313 to 1319 cm^{-1} attributed to the bending of the O−H group and strong interaction between the C=N functional group, respectively.[65] The absorption band appeared at 1120 cm^{-1} indicating that a redshift occurred due to a decrease in the wavenumber from 1143 to 1120 cm^{-1} attributing to the aliphatic chain.[54] The less intense peak observed at 870 cm^{-1} as compared to 880 cm^{-1} in pure MB indicates that a redshift occurs assigned to aromatic C−H bending.[66] Table S3 (Supporting Information) shows the summary of all the characteristic bands observed along with their wavenumber and functional groups.

2.4. HPLC- PDA Analysis of MB. Figure 7 shows the high-performance liquid chromatography (HPLC) chromatogram
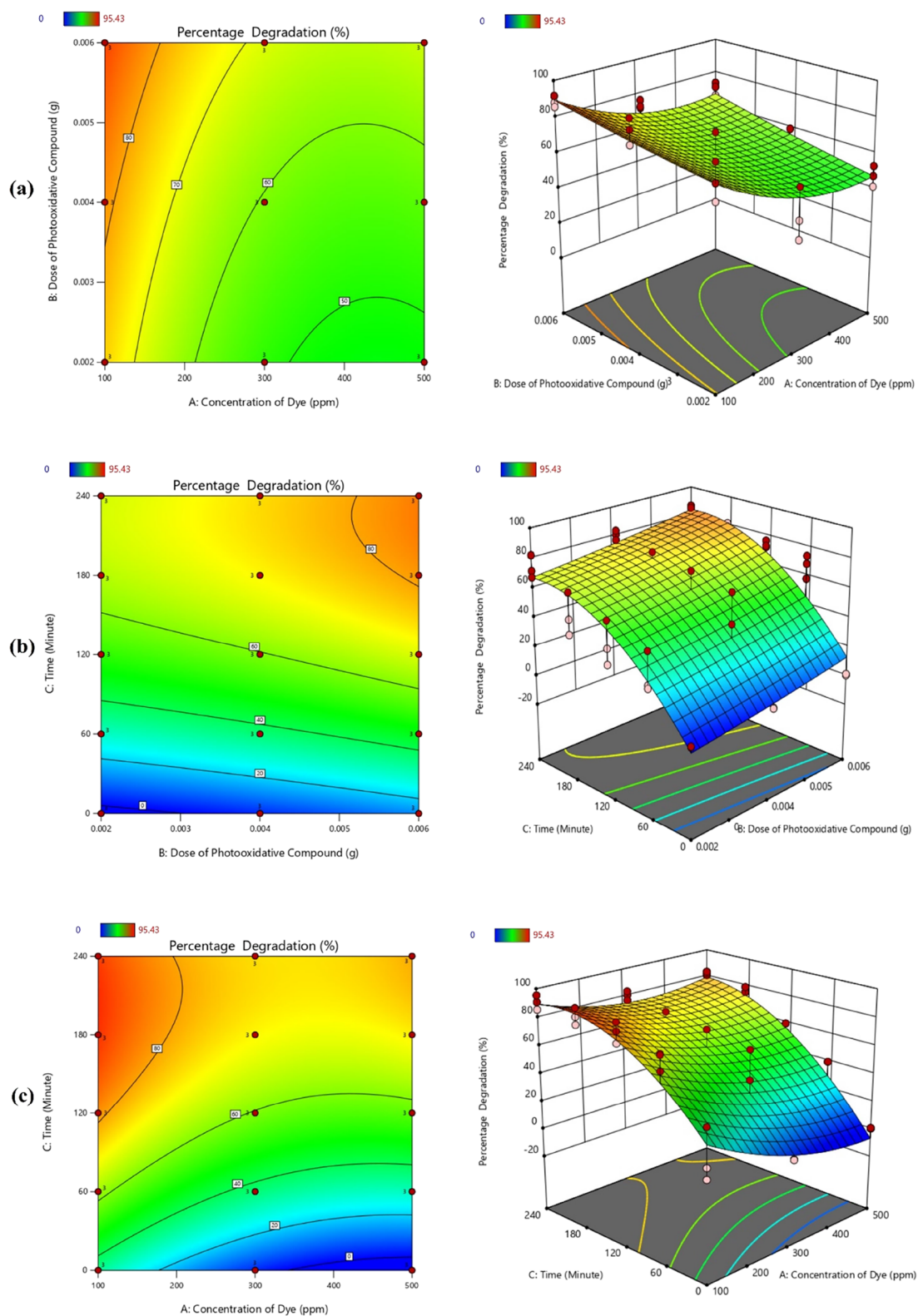
Figure 5. Response surface (3D) and contour plots (2D) for the percentage photooxidative degradation of MB as a function of (a) A: dye concentration (ppm) and B: dose of photooxidative compound (g) (at contact time = 120 min). (b) B: dose of photooxidative compound and C: time (minute) (dye concentration = 300 ppm and reaction time = 240 min) and (c) A: dye concentration (ppm) and C: time (minute): dose = 0.004 g; reaction time = 240 min.

of MB. Figure 7a illustrates the chromatogram of the degraded sample. Figure 7b shows a chromatogram of degraded samples at 254 nm. Figure 7c depicts a chromatogram of the pure dye sample at 670 nm. The HPLC chromatogram shows the

degradation of 1000 ppm MB by AA under 100 W of light for 4 h, recorded at 670 nm. In Figure 7a, two peaks were obtained at different retention times of 670 nm. **Peak A** at 1.954 min represents that the MB sample is degraded and a byproduct
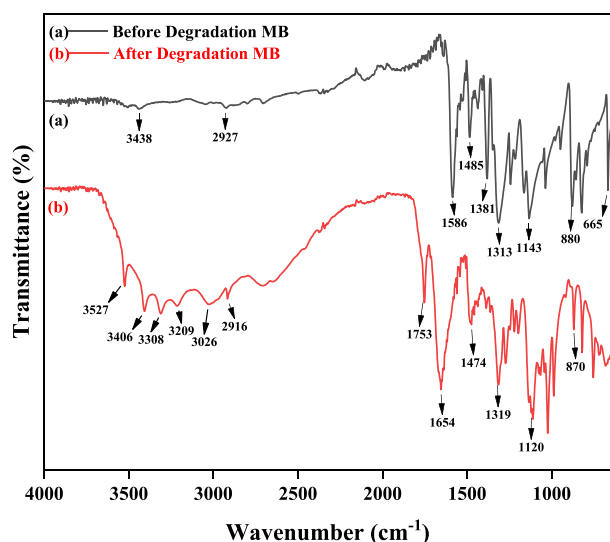
Figure 6. FT-IR spectra of MB (a) before and (b) after degradation.

was obtained. During the reaction, the N−C bond was destroyed between the N atom and the methyl group, observed by the conversion of dark-colored MB solution into a colorless form.[67] However, pure MB retention time was greater, as shown in Figure 7a, than that of **peak B**. This peak is seen after 240 min of irradiation and the **2nd peak B** can be visualized in Figure 7c; the degraded products are depicted in Figure 7b. These chromatographic variations provide evidence for the organophotocatalytic degradation of MB into aromatic amines. The presence of aromatic amines in the UV spectrum, specifically the peak of N3,N3,N7,N7-tetramethyl-10H-phenothiazine-3,7-diamine within the range of 254−259 nm, indicated that MB is entirely transformed into aromatic amines.[68]

2.5. GC-MS Analysis.

This investigation was done to unravel the chemical nature of metabolites produced from the organo-photooxidation of MB (5000 ppm) solution irradiated for 240 min with AA. GC-7890A and MS-5977A spectrometry (Agilent, USA) models were used for the identification of metabolites of MB degradation. Different degraded products were identified at 20.89 min of elution time as shown in Table 2 with their mass-to-charge (m/z) ratio. This also enabled the prediction of a suitable metabolic pathway for the degradation of MB as shown in Figure 9. The high-intensity peak is obtained in the gas chromatography−mass spectroscopy (GC−MS) spectrum of degraded MB. Figure 8 shows the mass spectrum of the identified intermediates at a retention time of 20.89 min. A series of chemical steps led to the degradation process, which produced a variety of degraded products. Furthermore, AA was a key reducing agent involved in transferring electrons, resulting in MB degradation.[69] Through the reduction of MB by AA, this transformation led to the oxidation of AA itself, which assisted in the reduction of other reactants. Electrons were transferred from AA to MB's electrophilic nitrogen. This electron transfer then led to the formation of leucomethylene blue (LMB) (m/z = 285), a crucial intermediate in the degradation process.[70] MB degradation was further elucidated by the formation of nitrated intermediates from protonated LMB in the presence of nitrating agents.[71] MB was identified as N3,N3,N7,N7-tetramethyl-10H-phenothiazine-3,7-diamine by searching the mass spectra library. Based on the GC−MS analysis, it was observed that C═N in the MB molecule oxidized to form C═O, in which AA may be involved, and the product 7-(dimethylamino)-3H-phenothiazine-3-one was obtained (m/z = 256). As shown in Figure 8, the intensity of the peak at (m/z = 285) notably decreased, and the appearance of a new peak has been observed. In the first reaction, sulfur is oxidized into sulfone, phenyl rings are hydroxylated, and MB is N-methylated. There is a possibility of being attacked by active
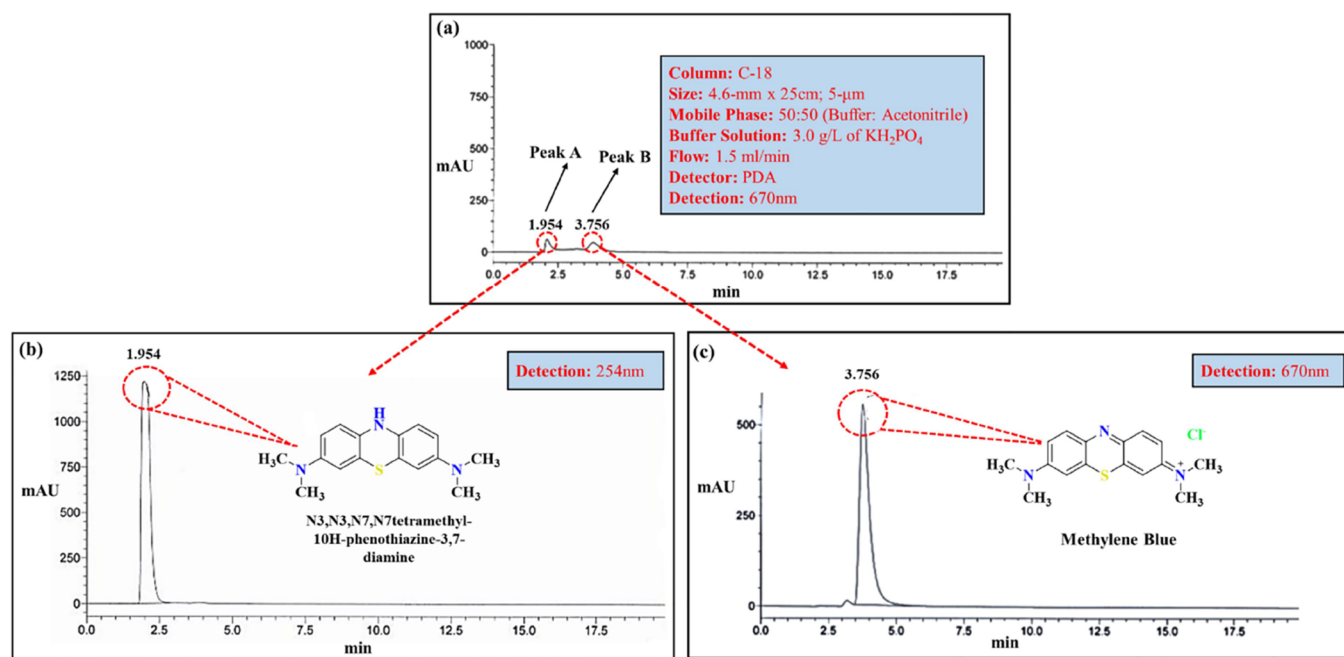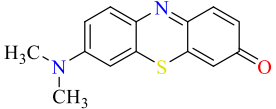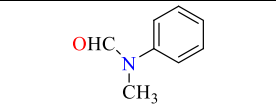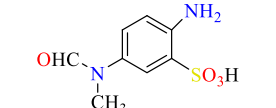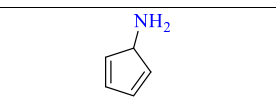

Figure 7. HPLC chromatogram showing the degradation of MB. In (a), the chromatogram illustrates the MB degraded sample. In (b), the chromatogram depicts MB after degradation at 254 nm. In (c), the chromatogram shows the peak before degradation at 670 nm.

Table 2. Literature-Supported Intermediate Products of MB Degradation

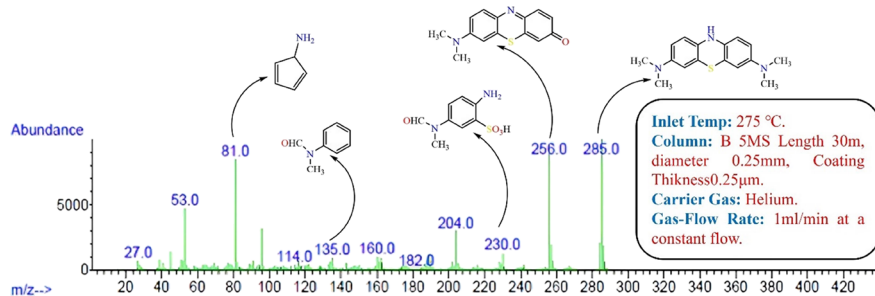| Sr.No	Intermediates Products	Chemical Names	Chemical Formula	m/z	Ref.
1		7-(dimethylamino)-3H-phenothiazin-3-one	$C_{14}H_{12}N_2OS$	256	72, 76
2		N-methyl-N-phenylformamide	C_8H_9NO	135	73
3		2-amino-5-(N-methylformamido)benzenesulfonic acid	$C_8H_{10}N_2O_4S$	230	72, 75
4		cyclopenta-2,4-dien-1-amine	C_5H_7N	81	74, 75

Figure 8. GC−MS spectrum mass peaks of organophoto-oxidatively degraded products of MB by AA.

OH.[72] When the dye molecule is photodegraded, the photogenerated holes and hydroxyl radicals preferentially attack the chromophore center. As a result of the amino group cleavage, hydrogen radical saturation, demethylation cleavage, release of one or more methyl group substituents on the amine groups, and further oxidation, products with $m/z =$ 230, 135, and 81 are formed.[72−74] H_2O and CO_2 are easily formed by oxidizing C=N and C−S bonds in MB.[74−76] Figure 9 shows the proposed pathway of degradation of MB by using AA as an organo-photooxidative compound based on GC-MS supported by HPLC.

2.6. GC−MS and HPLC Support the Proposed Degradation Mechanism of MB by AA. 2.7. Computational Details for the Supporting Mechanistic Study. The purposed mechanism of the MB degradation process is supported by this DFT study. The studied compounds were computed by Gaussian 09 program (1). The geometries of studied compounds were optimized using the B3LYP/6-31G (d,p) level basis set. The HOMO−LUMO bandgap energy and the contour of the molecular electrostatic potential (MEP) were also calculated at the same level of theory. Figure 10 illustrates the optimized structures of MB dye (a) and AA (b).

2.7.1. FMO Analysis. The reactivity of the molecules is explained by the energy gap between the HOMO and LUMO. Figure 11 shows the energies of the HOMO and LUMO and the band gap. The HOMO energy level correlates with nucleophilicity, while the LUMO energy level correlates with electrophilicity.[77] HOMO energy represents the ability to donate an electron, while the LUMO energy represents the ability to receive an electron. A large HOMO−LUMO gap indicates low reactivity and high chemical stability.[78] Kinetically, AA is more stable as compared to MB due to its large energy band gap (0.04662 eV), and MB is less stable due to the small energy gap (0.0425). The possibility of a chemical reaction between MB and AA can be described by the chemical potential (μ) values of the dye and acid. A molecule that has a small value of μ predicted more negative potential. This means more difficulty to lose an electron but easier to gain an electron.[79] The μ values of AA and MB are −0.21485 and −0.13952 eV, respectively. The low chemical stability and low ionization potential value of methylene predict that MB behaves as an acceptor in degradation reaction, while the high chemical stability and high chemical potential value of AA show that AA acts as a donor in reaction. The HOMO−LUMO, band gap energy, and chemical potential value of MB and AA are given in Table 3.

2.7.2. MEP Analysis. Electronic cloud surfaces, also known as MEPs,[80] consist of three zones: blue, red, and neutral. Green indicates neutral electrostatic potential, while blue means electron poor (strong positive electrostatic potential), and red means electron rich (weak negative electrostatic potential),[81,82] as shown in Figure 12. The potential increases from blue > green > yellow > orange > red.[77] The MEP surface of AA is shown in Figure 12a, which illustrates that the negative
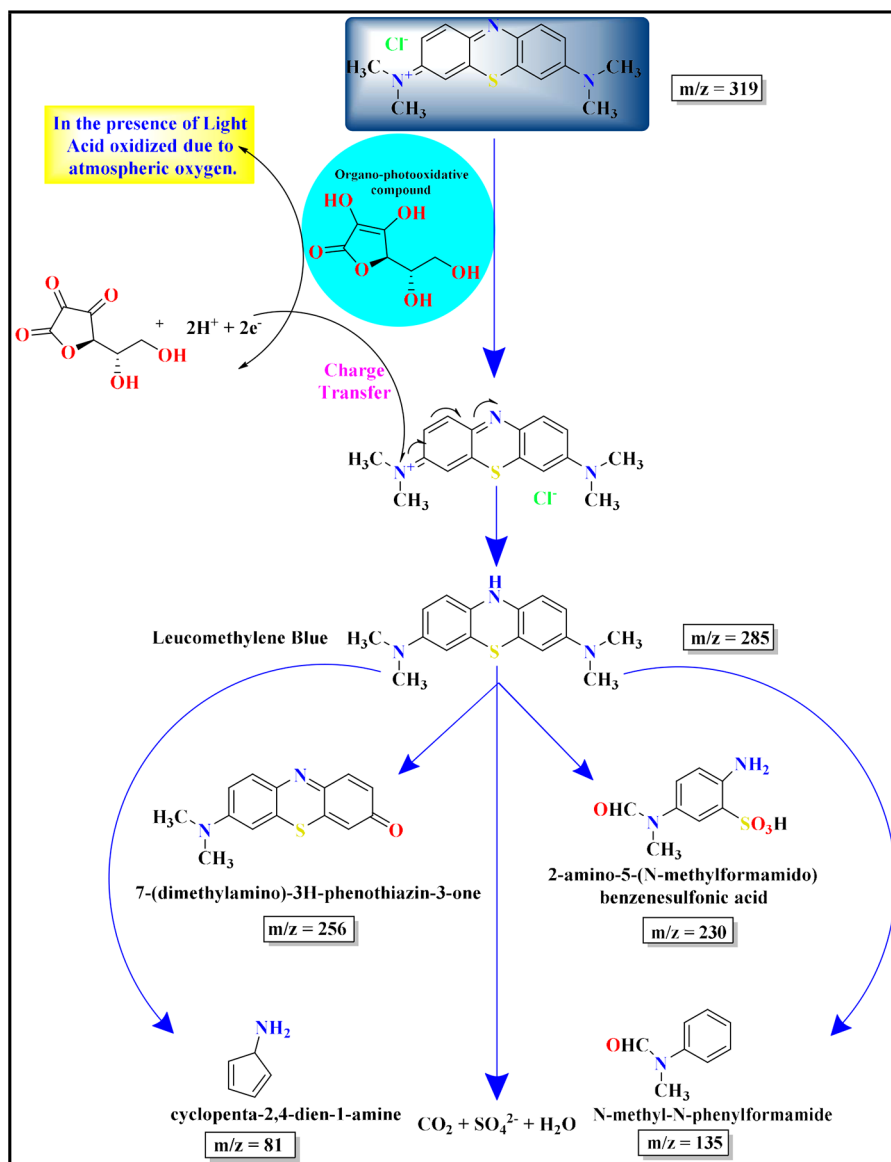
Figure 9. Proposed mechanism of MB degraded by AA was based on GC—MS.

electrostatic potential was scattered over oxygen atoms, and Figure 12b predicts that the blue electrostatic potential was found over all MB molecules. Accordingly, the nitrogen atom in MB is the site for nucleophilic attack, while oxygen atoms in AA are sites for electrophilic attack.

3. CONCLUSIONS

The area of organo-photooxidation is a frontier of research, offering new opportunities and transformative new reactions. In this study, the basic need to extend the attention of scientists toward a new, eco-friendly, and cost-effective approach was used to address the critical issue of MB degradation. It is a highly toxic compound that is often released by industrial processes and poses a significant environmental threat to aquatic ecosystems and potable water sources. AA was used as an organo-photooxidative compound for its degradation in the developed photocatalytic box. This research focuses on elucidating the impact of AA on the degradation of MB, in the presence of light, and its potential to enhance the degradation process. Remarkably,

results revealed a substantial increase in degradation efficiency, escalating from a modest 42% to an impressive 95% within a 240 min contact time. The optimal conditions for MB degradation were 0.004 g dosage of AA and 100 ppm concentration of MB at a contact time of 240 min with maximum efficiency. To substantiate these outcomes, an array of characterization techniques, including FT-IR, HPLC, GC-MS, and DFT studies, was employed to confirm the identity of the degraded products. LMB, a colorless product, was identified as a degraded product, confirmed by characterization techniques. Three variables were discussed by using the RSM statistical tool to optimize these parameters and further elevate the degradation efficiency. The degradation of various azo dyes such as reactive blue (RB), reactive black-5, eriochrome black T (EBT), and methyl orange (MO) was also done. In summary, the basic purpose of the study not only advances the understanding of the organo-photooxidation process but also underscores its potential as a sustainable and efficacious solution for wastewater treatment. This research contributes to
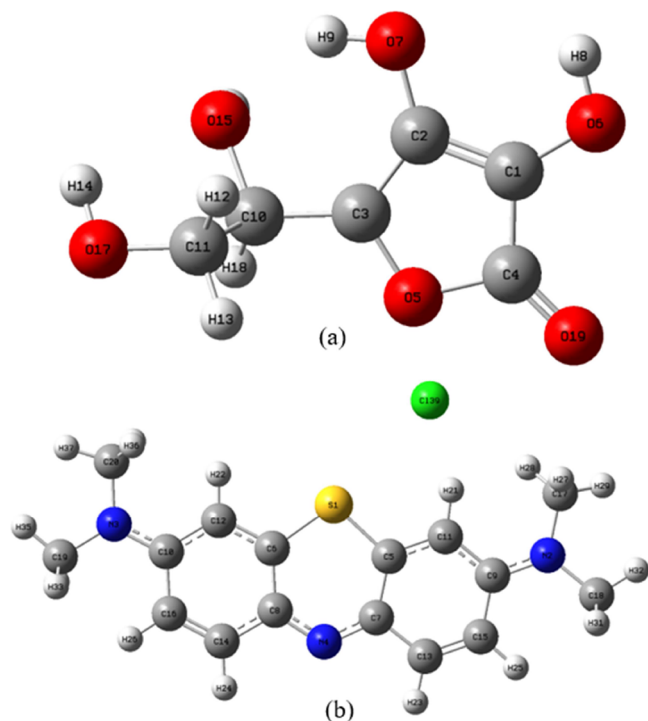
Figure 10. Optimized structures of (a) AA and (b) MB.

the ongoing pursuit of environmentally responsible strategies for safeguarding water quality and aquatic ecosystems.

4. MATERIALS AND METHODS

This study includes MB ($C_{16}H_{18}ClN_3S$), MO, EBT, RB, and reactive black-5 azo dyes and organo-photooxidative compounds such as AA ($C_6H_8O_6$), oxalic acid, tartaric acid, and citric acid of analytical grade, purchased by Sigma-Aldrich and used without further purification. For solution preparation, distilled water was used throughout the experiment. A photoreactor box was designed for the photooxidation process.

Table 3. Calculated HOMO-LUMO and Chemical Potential Value of AA (a) and MB (b)

molecules	E_{HOMO} (eV)	E_{LUMO} (eV)	μ (eV)
ascorbic acid	−0.23816	−0.19154	−0.21485
methylene blue	−0.16077	−0.11827	−0.13952

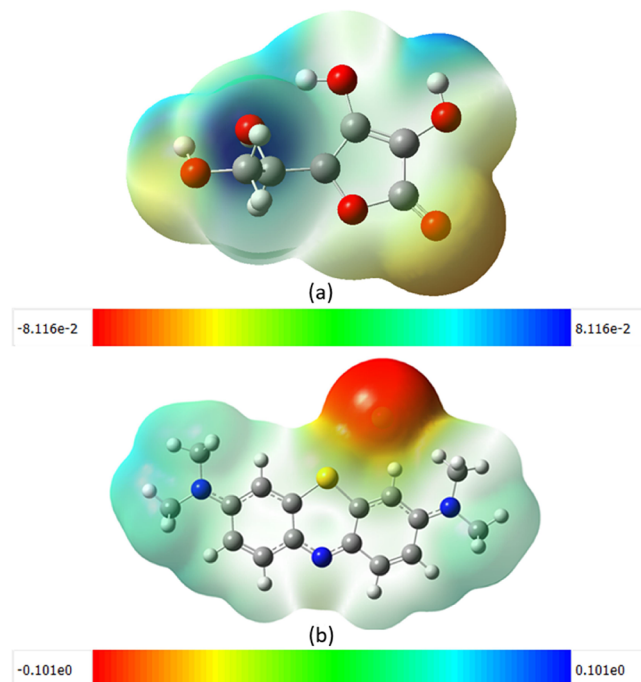**Figure 12.** Distribution of electron density on the optimized molecular geometries of AA (a) and MB (b).

Table S4 (Supporting Information) shows some chemical characteristics of MB.

4.1. Development of an Economical photoreactor Box for Photooxidation. The box includes a light source, which is essential for initiating photochemical reactions. It
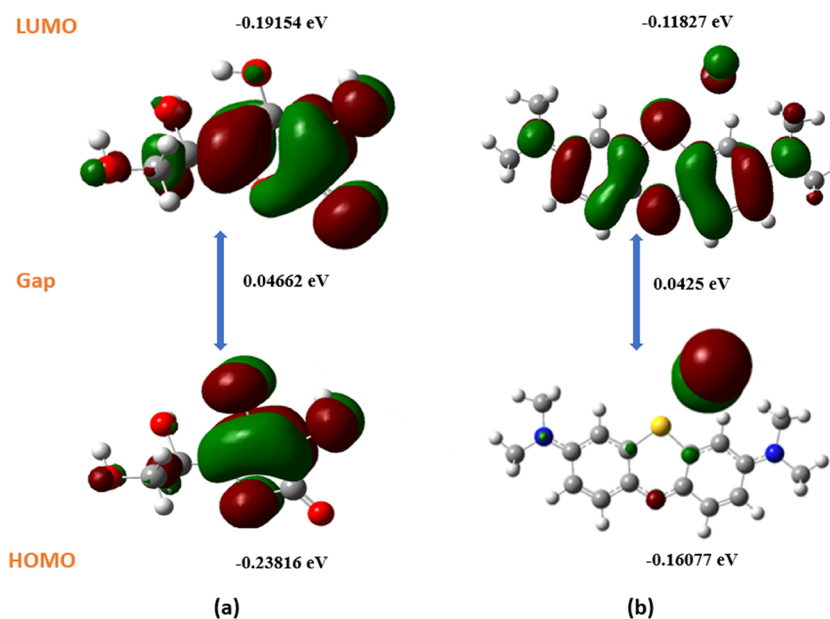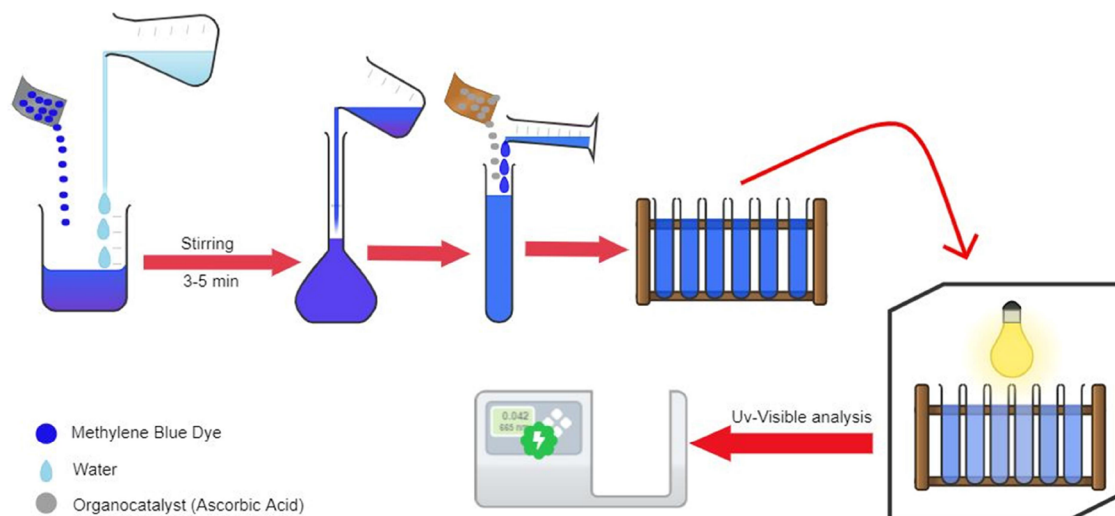

Figure 11. Pattern of the HOMO and LUMO frontier molecular orbital surfaces.

Scheme 1. Schematic Representation of the Activity of Organo-Photooxidation

consists of a 100 W tungsten filament bulb. The bulb is fitted centrally in the reactor box for effective light utilization. This photoreactor box was made from a cardboard box, having dimensions 13 × 12 × 14 in, wrapped from all sides with another sheet to prevent external light from interfering with the reaction. Coating the inner walls with aluminum foil enhances the enclosure's reflective properties, reducing the absorption of external heat or light. Moreover, the use of an aluminum foil lining in the box enhanced the symmetry of light within the box. The reflective nature of aluminum foil contributes to thermal insulation, acting as a barrier against dust, dirt, and other particulates from contacting the enclosed items or surfaces. This self-made photoreactor box includes monitoring features, allowing real-time observation of reaction parameters and progress. The specific design and components of the photoreactor box are eco-friendly and lightweight as shown in Figure S2 (Supporting Information).

4.2. Sample Preparation. In this study, the initial step involved washing all of the equipment with methanol and distilled water. Subsequently, different concentrations of MB were prepared in distilled water, including 100, 300, and 500 ppm. The degradation process was facilitated by introducing photooxidative compound doses of 0.002, 0.004, and 0.006 g, respectively, for each concentration of dye. After this, all the samples were put into the photoreactor box for degradation. For the analysis of the degraded material using HPLC and GC−MS, it was found that the concentration of MB needed to be higher, specifically at 5000 ppm, to analyze the material in powder form. On the other hand, the dose of the photo-oxidative compound for the organo-photooxidative process was kept at a minimum, with only 0.2 g being used. After sample degradation, the maximum amount of solvent was evaporated by using a rotary evaporator, which enables the removal of excess solvent and the acquisition of the desired powdered form for further analysis.

4.3. Organo-photooxidative Activity. The prepared samples of different concentrations were photooxidized using different doses of photooxidative compounds. There were three levels of sample concentration and three levels of photooxidative compound dose. To start the experiment, the mixture was stirred for 3−5 min after which the reaction mixture was exposed to visible light in a reactor box. The samples of MB were taken after 60, 120, 180, and 240 min,

respectively, and the absorbance of MB after each time interval was tested at 664 nm ($\lambda_{\max}$) using a UV−visible spectropho-tometer (VIS-1100). Similarly, the degradation process of all solutions of MB was determined with three replicate sets. The reference sample was also tested under the same conditions but without catalyst loading. Scheme 1 shows the activity of the organo-photooxidation process.

The degradation of the MB dye by using a photooxidative compound and its efficiency was determined by the following eq 1:

$$\text{Degradation Efficiency (DE)} = \frac{A_o - A}{A_o} \times 100 \tag{1}$$

A_o: initial absorbance of MB; A: final absorbance of MB; The optimal conditions for MB degradation from our study were 0.004 g of dosage from AA and 100 ppm concentration of MB at a contact time of 240 min.

4.4. Statistical Analysis and Response Surface Design. The response surface methodology (RSM) consists of mathematical and statistical tool, which is used to determine how various parameters affect the outcome.[45] According to RSM design principles, the CCD model was used to study and optimize the effects of three experimental factors on the percentage degradation efficiency of MB by using Stat-Ease Design Expert 13.0. The concentration of dye (ppm), dose of photooxidative compound (g), and reaction time (min) were calculated. A total of 135 experiments were conducted in this study. Three levels were defined for dye concentration and the dose of a photooxidative compound, while four levels were defined for time. These values were designed by the −1, 0, and +1 codes. To evaluate the outcome, analysis plots, coefficients of determination, and analyses of variance were used. When the P-value obtained is less than 0.05, the results are considered significant. The general form of the quadratic model is shown as follows in eq 2:

$$\eta = b_o + \sum_{i=1}^{n} b_i x_i + \sum_{i=1}^{n} b_{ii} x_i^2 + \sum_{i=1}^{n-1} \sum_{i=1}^{n} b_{ij} x_i x_j \tag{2}$$

where η is the response variable, b_o is the coefficient constant, b_i is a linear coefficient, b_{ii} is the quadratic coefficient, b_{ij} is the interaction coefficient, and the coded values are x_i and x_j of the parameters.[83,84,85]

Table 4. Experimental Ranges and Levels of the Effective Variables

factors	units	minimum	maximum	coded levels	
				coded low	coded high
concentration of dye	ppm	100.00	500.00	$-1 \leftrightarrow 100.00$	$+1 \leftrightarrow 500.00$
dose of photooxidative compound	g	0.0020	0.0060	$-1 \leftrightarrow 0.00$	$+1 \leftrightarrow 0.01$
irradiation time	min	0.0000	240.00	$-1 \leftrightarrow 0.00$	$+1 \leftrightarrow 240.00$

$$\% \ (\eta) = 59.42 + (-12.73)X_1 + (8.28)X_2 + (35.42)X_3$$
$$+ (1.51)X_1X_2 + (7.64)X_1X_3 + (-0.11)X_2X_3$$
$$+ (9.66)X_1^2 + (0.85)X_2^2 + (-20.14)X_3^2 \qquad (3)$$

In eq 3, % (η) is the percentage degradation response, and X_1, X_2, and X_3 are the corresponding independent parameters such as concentration of dye (ppm), dose of photooxidative compound (g), and reaction time (min) respectively.

By using ANOVA, regression factor values were measured. An established predictive model was evaluated using the correlation coefficient R^2, modified R^2, p-value, and lack of fit to assess its validity and suitability. Independent variables were assessed by using the 95% confidence level to determine their relevance to the MB degradation process.

4.4.1. Factors Affecting Different Levels and Their Significance. The designed statistical model is used to determine which coefficient does not influence each of the responses. It is possible to improve the quality of statistical models by removing coefficients that do not affect all responses. The experimental ranges and levels of the effective variables are listed in Table 4.

4.5. Computational Study. In the first step, chemical structures of the dye and acid were drawn and files were saved using Gauss view 6.0.[86] Then, we added the instructions for DFT calculations. The job type basis set, calculation method, functionals, and keywords were selected.[87] Based on the 6-31G (d,p) basis set, MB and AA were optimized using DFT with the B3LYP functional (44).[88] All the calculations were done in Gaussian 09[89] after the file was terminated normally, and the result files/log files were analyzed again in Gauss view 6.0.[90] The optimized structures were calculated from log files and the HOMO−LUMO values from CHK files.[91] An optimized geometry of the compounds was used to develop the MEP surface.[92]

ASSOCIATED CONTENT

Ⓢ Supporting Information

The Supporting Information is available free of charge at https://pubs.acs.org/doi/10.1021/acsomega.3c09989.

> Chemical structures of dye and sample; photoreactor box; central composite design matrix; characteristic bands; chemical characteristics; wavelength-dependent optical density; and determination of optical density (PDF)

AUTHOR INFORMATION

Corresponding Author

Muhammad Adnan Iqbal − *Department of Chemistry and Synthetic Organometallic and Coordination Chemistry Laboratory, University of Agriculture Faisalabad, Faisalabad 38000, Pakistan;* ⓞ orcid.org/0000-0001-6241-7547; Email: adnan.iqbal@uaf.edu.pk

Authors

Adnan Majeed − *Department of Chemistry, University of Agriculture Faisalabad, Faisalabad 38000, Pakistan*

Ahmad H. Ibrahim − *Pharmacy Department, Faculty of Pharmacy, Tishk International University, Erbil, KRG, Iraq*

Sawsan S. Al-Rawi − *Biology Education Department, Faculty of Education, Tishk International University, Erbil, KRG, Iraq*

Muhammad Kashif − *Department of Mathematics and Statistics, University of Agriculture Faisalabad, Faisalabad 38000, Pakistan*

Muhammad Yousif − *Department of Chemistry, University of Agriculture Faisalabad, Faisalabad 38000, Pakistan*

Zain Ul Abidin − *Department of Chemistry, University of Agriculture Faisalabad, Faisalabad 38000, Pakistan*

Shahzaib Ali − *Department of Chemistry, University of Agriculture Faisalabad, Faisalabad 38000, Pakistan*

Muhammad Arbaz − *Department of Chemistry, University of Agriculture Faisalabad, Faisalabad 38000, Pakistan*

Syed Arslan Hussain − *Department of Chemistry, University of Agriculture Faisalabad, Faisalabad 38000, Pakistan*

Complete contact information is available at:
https://pubs.acs.org/10.1021/acsomega.3c09989

Author Contributions

A.M.: writing-original draft, Investigation, and Software. A.H.I.: resources. S.S.A.: validation. M.A.I.: conceptualization, resources, supervision, and overall guidance. M.K.: data curation and visualization. M.Y.: review and editing and data curation. Z.U.A.: formal analysis. S.A.: validation and data curation. M.A.: review and editing. S.A.H.: validation and review.

Notes

The authors declare no competing financial interest.

REFERENCES

(1) Wang, C.-C.; Li, J.-R.; Lv, X.-L.; Zhang, Y.-Q.; Guo, G. Photocatalytic organic pollutants degradation in metal−organic frameworks. *Energy Environ. Sci.* **2014**, 7 (9), 2831−2867. Pinto, V. L.; Cervantes, T. N. M.; Soto, P. C.; Sarto, G.; Bessegato, G. G.; Almeida, L. C. D. Multivariate optimization of methylene blue dye degradation using electro-Fenton process with self-doped TiO2 nanotube anode. *Chemosphere* **2023**, 344, No. 140336.

(2) Estrada, M.; Sepúlveda, F.; Nenen, A.; Bravo-Linares, C.; Nishide, H.; Suga, T.; Moreno-Villoslada, I. Novel reusable catalytic poly(4-styrenesulfonate-co-glycidylmethacrylate) foams for adsorption and photodegradation of the model pollutant dye methylene blue

based on aromatic-aromatic interactions. *Chemical Engineering Journal* **2023**, *459*, No. 141518.

(3) Salama, A.; Mohamed, A.; Aboamera, N. M.; Osman, T.; Khattab, A. Photocatalytic degradation of organic dyes using composite nanofibers under UV irradiation. *Applied Nanoscience* **2018**, *8*, 155−161. Nie, Y.; Zhang, Y.; Nie, X.; Tian, X.; Dai, C.; Shi, J. Colloidal iron species driven enhanced H2O2 decomposition into hydroxyl radicals for efficient removal of methylene blue from water. *Journal of Hazardous Materials* **2023**, *448*, No. 130949.

(4) Khan, A.; Roy, A.; Bhasin, S.; Emran, T. B.; Khusro, A.; Eftekhari, A.; Moradi, O.; Rokni, H.; Karimi, F. Nanomaterials: An alternative source for biodegradation of toxic dyes. *Food Chem. Toxicol.* **2022**, *164*, 112996.

(5) Wang, S.; Gao, H.; Fang, L.; Hu, Q.; Sun, G.; Chen, X.; Yu, C.; Tang, S.; Yu, X.; Zhao, X. Synthesis of novel CQDs/CeO$_2$/SrFe$_{12}$O$_{19}$ magnetic separation photocatalysts and synergic adsorption-photocatalytic degradation effect for methylene blue dye removal. *Chem. Eng. J. Adv.* **2021**, *6*, No. 100089.

(6) Srivastava, N.; Majumder, C. Novel biofiltration methods for the treatment of heavy metals from industrial wastewater. *Journal of hazardous materials* **2008**, *151* (1), 1−8. Guo, Z.; Ren, P.; Wang, J.; Hou, X.; Tang, J.; Liu, Z.; Chen, Z.; Jin, Y.; Ren, F. Methylene blue adsorption derived thermal insulating N, S-co-doped TiC/carbon hybrid aerogel for high-efficient absorption-dominant electromagnetic interference shielding. *Chemical Engineering Journal* **2023**, *451*, No. 138667.

(7) Ajiboye, T. O.; Oyewo, O. A.; Onwudiwe, D. C. Simultaneous removal of organics and heavy metals from industrial wastewater: A review. *Chemosphere* **2021**, *262*, No. 128379.

(8) Yang, G.; Tang, L.; Zeng, G.; Cai, Y.; Tang, J.; Pang, Y.; Zhou, Y.; Liu, Y.; Wang, J.; Zhang, S. Simultaneous removal of lead and phenol contamination from water by nitrogen-functionalized magnetic ordered mesoporous carbon. *Chem. Eng. J.* **2015**, *259*, 854−864.

(9) Bibi, S.; Shah, S. S.; Muhammad, F.; Siddiq, M.; Kiran, L.; Aldossari, S. A.; Mushab, M. S. S.; Sarwar, S. Cu-doped mesoporous TiO$_2$ photocatalyst for efficient degradation of organic dye via visible light photocatalysis. *Chemosphere* **2023**, *339*, No. 139583.

(10) Oladoye, P. O.; Ajiboye, T. O.; Omotola, E. O.; Oyewola, O. J. Methylene blue dye: Toxicity and potential technologies for elimination from (waste) water. *Results in Engineering* **2022**, *16*, 100678.

(11) Khajone, V. B.; Balinge, K. R.; Patle, D. S.; Bhagat, P. R. Synthesis and characterization of polymer supported Fe-phthalocyanine entangled with carboxyl functionalized benzimidazolium moiety: a heterogeneous catalyst for efficient visible-light-driven degradation of organic dyes from aqueous solutions. *J. Mol. Liq.* **2019**, *288*, 111032.

(12) Chahar, D.; Taneja, S.; Bisht, S.; Kesarwani, S.; Thakur, P.; Thakur, A.; Sharma, P. Photocatalytic activity of cobalt substituted zinc ferrite for the degradation of methylene blue dye under visible light irradiation. *J. Alloys Compd.* **2021**, *851*, No. 156878.

(13) Shariati, M.; Babaei, A.; Azizi, A. Synthesis of Ag2CrO4/Ag/Fe3O4/RGO nanocomposite as a suitable photocatalyst for degradation of methylene blue in aqueous media: RSM modeling, kinetic and energy consumption studies. *Inorg. Chem. Commun.* **2022**, *145*, No. 110004.

(14) Chen, M.-L.; Li, S.-S.; Wen, L.; Xu, Z.; Li, H.-H.; Ding, L.; Cheng, Y.-H. Exploration of double Z-type ternary composite long-afterglow/graphitic carbon nitride@ metal−organic framework for photocatalytic degradation of methylene blue. *J. Colloid Interface Sci.* **2023**, *629*, 409−421. Cheng, L.; Zhang, Y.; Fan, W.; Ji, Y. Synergistic adsorption-photocatalysis for dyes removal by a novel biochar−based Z-scheme heterojunction BC/2ZIS/WO3: Mechanistic investigation and degradation pathways. *Chemical Engineering Journal* **2022**, *445*, No. 136677.

(15) Lo, J. C.; Darracq, M. A.; Clark, R. F. A review of methylene blue treatment for cardiovascular collapse. *Journal of emergency medicine* **2014**, *46* (5), 670−679.

(16) Bapat, P.; Nandy, S. K.; Wangikar, P.; Venkatesh, K. Quantification of metabolically active biomass using methylene blue dye reduction test (MBRT): measurement of CFU in about 200 s. *J. Microbiol. Methods* **2006**, *65* (1), 107−116.

(17) Chung, D. C. K.; Lin, E. S.; Peng, L.; Jiang, X.; Ong, J. W.; Abid, H. A.; Song, Z.; Liew, O. W.; Ng, T. W. Efficient drop reactor processing of methylene blue degradation with silver nanowire catalysts. *Colloids Surf., A* **2021**, *610*, No. 125749.

(18) Oladoye, P. O.; Ajiboye, T. O.; Omotola, E. O.; Oyewola, O. J. Methylene blue dye: Toxicity and potential elimination technology from wastewater. *Results in Engineering* **2022**, *16*, No. 100678.

(19) Lyu, H.; Gao, B.; He, F.; Zimmerman, A. R.; Ding, C.; Tang, J.; Crittenden, J. C. Experimental and modeling investigations of ball-milled biochar for the removal of aqueous methylene blue. *Chemical Engineering Journal* **2018**, *335*, 110−119. Yao, X.; Fang, Y.; Guo, Y.; Xu, M. Degradation of methylene blue using a novel gas-liquid hybrid DDBD reactor: Performance and pathways. *Chemosphere* **2023**, *336*, No. 139172. Ahmad, R.; Kumar, R. Adsorption studies of hazardous malachite green onto treated ginger waste. *Journal of environmental management* **2010**, *91* (4), 1032−1038.

(20) Moorthy, A. K.; Rathi, B. G.; Shukla, S. P.; Kumar, K.; Bharti, V. S. Acute toxicity of textile dye Methylene blue on growth and metabolism of selected freshwater microalgae. *Environ. Toxicol. Pharmacol.* **2021**, *82*, No. 103552.

(21) Dos Santos, A. B.; Cervantes, F. J.; Van Lier, J. B. Review paper on current technologies for decolourisation of textile wastewaters: perspectives for anaerobic biotechnology. *Bioresource technology* **2007**, *98* (12), 2369−2385.

(22) Mohammed, M.; Shitu, A.; Ibrahim, A. Removal of methylene blue using low cost adsorbent: a review. *Res. J. Chem. Sci.* **2014**, *4*, 91.

(23) Lafi, R.; Gzara, L.; Lajimi, R. H.; Hafiane, A. Treatment of textile wastewater by a hybrid ultrafiltration/electrodialysis process. *Chemical Engineering and Processing-Process Intensification* **2018**, *132*, 105−113.

(24) Kang, H.; Shi, J.; Liu, L.; Shan, M.; Xu, Z.; Li, N.; Li, J.; Lv, H.; Qian, X.; Zhao, L. Sandwich morphology and superior dye-removal performances for nanofiltration membranes self-assemblied via graphene oxide and carbon nanotubes. *Appl. Surf. Sci.* **2018**, *428*, 990−999. Nadeem, N.; Yaseen, M.; Rehan, Z. A.; Zahid, M.; Shakoor, R. A.; Jilani, A.; Iqbal, J.; Rasul, S.; Shahid, I. Coal fly ash supported CoFe2O4 nanocomposites: Synergetic Fenton-like and photocatalytic degradation of methylene blue. *Environmental Research* **2022**, *206*, No. 112280.

(25) Patel, P.; Maliekal, P.; Lingayat, S.; Badani, P. Understanding the Kinetics and Reduction of Methylene Blue Using NaBH4. *Russian Journal of Physical Chemistry B* **2022**, *16* (5), 869−876. Ihaddaden, S.; Aberkane, D.; Boukerroui, A.; Robert, D. Removal of methylene blue (basic dye) by coagulation-flocculation with biomaterials (bentonite and Opuntia ficus indica). *Journal of Water Process Engineering* **2022**, *49*, No. 102952.

(26) Panizza, M.; Barbucci, A.; Ricotti, R.; Cerisola, G. Electrochemical degradation of methylene blue. *Sep. Purif. Technol.* **2007**, *54* (3), 382−387.

(27) Mohammadpour, A.; Karami, N.; Zabihi, R.; Fazeliyan, E.; Abbasi, A.; Karimi, S.; Barbosa de Farias, M.; Adeodato Vieira, M. G.; Shahsavani, E.; Mousavi Khaneghah, A. Green synthesis, characterization, and application of Fe3O4 nanoparticles for methylene blue removal: RSM optimization, kinetic, isothermal studies, and molecular simulation. *Environmental Research* **2023**, *225*, No. 115507.

(28) Gao, L.; Zhai, Y.; Ma, H.; Wang, B. Degradation of cationic dye methylene blue by ozonation assisted with kaolin. *Appl. Clay Sci.* **2009**, *46* (2), 226−229.

(29) Jiang, T.; Wang, B.; Gao, B.; Cheng, N.; Feng, Q.; Chen, M.; Wang, S. Degradation of organic pollutants from water by biochar-assisted advanced oxidation processes: Mechanisms and applications. *Journal of Hazardous Materials* **2023**, *442*, No. 130075.

(30) Alkaykh, S.; Mbarek, A.; Ali-Shattle, E. E. Photocatalytic degradation of methylene blue dye in aqueous solution by MnTiO$_3$

nanoparticles under sunlight irradiation. *Heliyon* **2020**, *6* (4), No. e03663, DOI: 10.1016/j.Heliyon.2020.e03663.

(31) Hu, W.; Liu, D.; Su, S.; Ren, L.; Ren, H.; Wei, L.; Yue, S.; Xie, Q.; Zhang, Z.; Wang, Z. Photochemical degradation of organic matter in the atmosphere. *Adv. Sustainable Syst.* **2021**, *5* (11), No. 2100027.

(32) Sharma, R.; Kumar, V.; Bansal, S.; Singhal, S. Assortment of magnetic nanospinels for activation of distinct inorganic oxidants in photo-Fenton's process. *J. Mol. Catal. A: Chem.* **2015**, *402*, 53–63.

(33) Guo, X.; Wang, K.; Xu, Y. Tartaric acid enhanced CuFe2O4-catalyzed heterogeneous photo-Fenton-like degradation of methylene blue. *Materials Science and Engineering: B* **2019**, *245*, 75–84.

(34) Vega-Peñaloza, A.; Mateos, J.; Companyó, X.; Escudero-Casao, M.; Dell'Amico, L. A Rational Approach to Organo-Photocatalysis: Novel Designs and Structure-Property Relationships. *Angew. Chem., Int. Ed.* **2021**, *60* (3), 1082–1097. Ghatge, S.; Yang, Y.; Ko, Y.; Yoon, Y.; Ahn, J.-H.; Kim, J. J.; Hur, H.-G. Degradation of sulfonated polyethylene by a bio-photo-fenton approach using glucose oxidase immobilized on titanium dioxide. *Journal of Hazardous Materials* **2022**, *423*, No. 127067.

(35) Sahoo, B. M.; Banik, B. K. Organocatalysis: trends of drug synthesis in medicinal chemistry. *Current Organocatalysis* **2019**, *6* (2), 92–105.

(36) Volla, C. M.; Atodiresei, I.; Rueping, M. Catalytic C–C bond-forming multi-component cascade or domino reactions: Pushing the boundaries of complexity in asymmetric organocatalysis. *Chem. Rev.* **2014**, *114* (4), 2390–2431.

(37) Lyu, J.; Claraz, A.; Vitale, M. R.; Allain, C.; Masson, G. Preparation of Chiral Photosensitive Organocatalysts and their Application for the Enantioselective Synthesis of 1, 2-diamines. *Journal of Organic Chemistry* **2020**, *85* (20), 12843–12855.

(38) Hargittai, I. The 2021 chemistry Nobel laureates and asymmetric organocatalysis. *Structural Chemistry* **2022**, *33* (1), 303–305.

(39) Rogers, D. A.; Hopkins, M. D.; Rajagopal, N.; Varshney, D.; Howard, H. A.; LeBlanc, G.; Lamar, A. A. US Food and Drug Administration-Certified Food Dyes as Organocatalysts in the Visible Light-Promoted Chlorination of Aromatics and Heteroaromatics. *ACS omega* **2020**, *5* (13), 7693–7704.

(40) Khan, I.; Saeed, K.; Zekker, I.; Zhang, B.; Hendi, A. H.; Ahmad, A.; Ahmad, S.; Zada, N.; Ahmad, H.; Shah, L. A. Review on methylene blue: Its properties, uses, toxicity and photodegradation. *Water* **2022**, *14* (2), 242.

(41) Ghaemi, A.; Darabi, H. R.; Aghapoor, K.; Mohsenzadeh, F.; Sayahi, H.; Taherzadeh, H.; Mojdehi, M. F.; Balavar, Y.; Farhangian, H. Ascorbic acid as a multifunctional hydrogen bonding catalyst for Paal–Knorr synthesis of N-substituted mono-and bis-pyrroles: experimental and theoretical aspects. *Res. Chem. Intermed.* **2023**, *49*, 1–16.

(42) Das, A.; Yadav, R. N.; Banik, B. K. Ascorbic acid-mediated reactions in organic synthesis. *Current Organocatalysis* **2020**, *7* (3), 212–241.

(43) Karuppasamy, P.; Nisha, N. R. N.; Pugazhendhi, A.; Kandasamy, S.; Pitchaimuthu, S. An investigation of transition metal doped TiO2 photocatalysts for the enhanced photocatalytic decoloration of methylene blue dye under visible light irradiation. *J. Environ. Chem. Eng.* **2021**, *9* (4), No. 105254.

(44) Bibi, S.; Ahmad, A.; Anjum, M. A. R.; Haleem, A.; Siddiq, M.; Shah, S. S.; Al Kahtani, A. Photocatalytic degradation of malachite green and methylene blue over reduced graphene oxide (rGO) based metal oxides (rGO-Fe3O4/TiO2) nanocomposite under UV-visible light irradiation. *J. Environ. Chem. Eng.* **2021**, *9* (4), No. 105580.

(45) Ananda, A.; Ramakrishnappa, T.; Ravishankar, T.; Reddy Yadav, L.; Jayanna, B. RSM-BBD optimization approach for degradation and electrochemical sensing of Evan's blue dye using green synthesized ZrO2–ZnO nanocomposite. *Inorganic and Nano-Metal Chemistry* **2023**, 1–15.

(46) Srivastava, S.; Garg, R. Process parameter optimization of gas metal arc welding on IS: 2062 mild steel using response surface methodology. *Journal of Manufacturing Processes* **2017**, *25*, 296–305.

(47) Salehi, K.; Bahmani, A.; Shahmoradi, B.; Pordel, M.; Kohzadi, S.; Gong, Y.; Guo, H.; Shivaraju, H.; Rezaee, R.; Pawar, R. Response surface methodology (RSM) optimization approach for degradation of Direct Blue 71 dye using CuO–ZnO nanocomposite. *Int. J. Environ. Sci. Technol.* **2017**, *14*, 2067–2076.

(48) Malika, M.; Sonawane, S. S. Statistical modelling for the Ultrasonic photodegradation of Rhodamine B dye using aqueous based Bi-metal doped TiO2 supported montmorillonite hybrid nanofluid via RSM. *Sustainable Energy Technologies and Assessments* **2021**, *44*, 100980.

(49) Zuorro, A.; Fidaleo, M.; Lavecchia, R. Response surface methodology (RSM) analysis of photodegradation of sulfonated diazo dye Reactive Green 19 by UV/H2O2 process. *J. Environ. Manage.* **2013**, *127*, 28–35.

(50) Da Silva, R. A.; Guerra, D. J. Use of natural and modified kaolinite/ilite as adsorbent for removal methylene blue dye from aqueous solution. *Journal of the Chilean Chemical Society* **2013**, *58* (1), 1517–1519. Hevira, L.; Ighalo, J. O.; Aziz, H.; Zein, R. Terminalia catappa shell as low-cost biosorbent for the removal of methylene blue from aqueous solutions. *J. Ind. Eng. Chem.* **2021**, *97*, 188–199.

(51) Ganapuram, B. R.; Alle, M.; Dadigala, R.; Dasari, A.; Maragoni, V.; Guttena, V. Catalytic reduction of methylene blue and Congo red dyes using green synthesized gold nanoparticles capped by salmalia malabarica gum. *International Nano Letters* **2015**, *5*, 215–222.

(52) Basker, A.; Shabudeen, S.; Shekhar, A. P.; Daniel, S. Validating Adsorptive Capacity of Areca Husk Carbon onto Methylene Blue with ANOVA Modeling. *Chiang Mai J. Sci.* **2016**, *43* (1), 183–194.

(53) Elmaghraby, N. A.; Omer, A. M.; Kenawy, E.-R.; Gaber, M.; Hassaan, M. A.; Ragab, S.; Hossain, I.; El Nemr, A. Electrospun cellulose acetate/activated carbon composite modified by EDTA (rC/AC-EDTA) for efficient methylene blue dye removal. *Sci. Rep.* **2023**, *13* (1), 9919.

(54) Ovchinnikov, O. V.; Evtukhova, A. V.; Kondratenko, T. S.; Smirnov, M. S.; Khokhlov, V. Y.; Erina, O. V. Manifestation of intermolecular interactions in FTIR spectra of methylene blue molecules. *Vib. Spectrosc.* **2016**, *86*, 181–189.

(55) El-Sakhawy, M.; Mohamed, S.; Salama, A.; Sarhan, H.-A. Preparation and infrared study of cellulose based amphiphilic materials. *Cellul. Chem. Technol.* **2018**, *52*, 193–200.

(56) BinSabt, M.; Sagar, V.; Singh, J.; Rawat, M.; Shaban, M. Green synthesis of CS-TiO2 NPs for efficient photocatalytic degradation of methylene blue dye. *Polymers* **2022**, *14* (13), 2677.

(57) Türkeş, E.; Sağ Açıkel, Y. Synthesis and characterization of magnetic halloysite–chitosan nanocomposites: use in the removal of methylene blue in wastewaters. *International Journal of Environmental Science and Technology* **2020**, *17* (3), 1281–1294.

(58) Xia, Y.; Yao, Q.; Zhang, W.; Zhang, L.; Zhang, Z.; Zhao, M. Comparative adsorption of methylene blue by magnetic baker's yeast and EDTAD-modified magnetic baker's yeast: Equilibrium and kinetic study. *Arabian J. Chem.* **2019**, *12*, 2448 DOI: 10.1016/j.arabjc.2015.03.010.

(59) Dassanayake, R. S.; Rajakaruna, E.; Abidi, N. Borax-cross-linked guar gum-manganese dioxide composites for oxidative decolorization of methylene blue. *J. Nanomater.* **2019**, *2019*. DOI: 1.

(60) Prabakaran, E.; Velempini, T.; Molefe, M.; Pillay, K. Comparative study of KF, KCl and KBr doped with graphitic carbon nitride for superior photocatalytic degradation of methylene blue under visible light. *Journal of Materials Research and Technology* **2021**, *15*, 6340–6355.

(61) Yu, Y.; Zhao, X.; Ye, L. Poly (vinyl alcohol)/graphene oxide nanocomposite hydrogel with catalytic activity: the removal behavior and dual adsorption/catalytic degradation mechanism for dye wastewater. *Polym. Int.* **2021**, *70* (3), 331–340.

(62) Soury, R.; Teka, S.; Alenezi, K. M.; Jabli, M. Characterization and application of ligno-cellulosic fibers derived from Robinia Pseudoacacia for the bio-sorption of methylene blue from water. *International Journal of Phytoremediation* **2023**, *25* (10), 1359–1370. Xiao, L.-P.; Shi, Z.-J.; Xu, F.; Sun, R.-C.; Amar, K. M. Structural characterization of lignins isolated from Caragana sinica using FT-IR

and NMR spectroscopy. *Spectrosc. Spectral Anal.* **2011**, *31* (9), 2369−2376.

(63) Li, X.; Ni, C.; Yao, C.; Chen, Z. Development of attapulgite/Ce1− xZrxO2 nanocomposite as catalyst for the degradation of methylene blue. *Applied Catalysis B: Environmental* **2012**, *117*, 118−124.

(64) Yu, J.-X.; Li, B.-H.; Sun, X.-M.; Yuan, J.; Chi, R.-A. Polymer modified biomass of baker's yeast for enhancement adsorption of methylene blue, rhodamine B and basic magenta. *Journal of Hazardous Materials* **2009**, *168* (2−3), 1147−1154.

(65) Shi, Y.; Baker, J.; Feng, C.; Wang, X.; Li, Z. Removal of toluidine blue from water using 1:1 layered clay minerals. *Advanced Powder Technology* **2022**, *33* (6), No. 103608. Van Damme, H.; Crespin, M.; Cruz, M.; Fripiat, J. Adsorption of safranine by Na+, Ni 2+ and Fe 3+ montmorillonites. *Clays and Clay Minerals* **1977**, *25*, 19−25. Shi, Y.; Wang, X.; Wang, X.; Carlson, K.; Li, Z. Removal of toluidine blue and safranin O from single and binary solutions using zeolite. *Crystals* **2021**, *11* (10), 1181.

(66) Huang, W.; Chen, J.; Zhang, J. Adsorption characteristics of methylene blue by biochar prepared using sheep, rabbit and pig manure. *Environmental Science and Pollution Research* **2018**, *25*, 29256−29266.

(67) Fong, W.; Affam, A.; Chung, W. Synthesis of Ag/Fe/CAC for colour and COD removal from methylene blue dye wastewater. *International journal of environmental science and technology* **2020**, *17* (7), 3485−3494.

(68) Pinheiro, H. M.; Touraud, E.; Thomas, O. Aromatic amines from azo dye reduction: status review with emphasis on direct UV spectrophotometric detection in textile industry wastewaters. *Dyes Pigm.* **2004**, *61* (2), 121−139. Katafias, A.; Lipińska, M.; Strutyński, K. Alkaline hydrogen peroxide as a degradation agent of methylene blue—kinetic and mechanistic studies. *Reaction Kinetics, Mechanisms and Catalysis* **2010**, *101* (2), 251−266.

(69) Messih, M. A.; Ahmed, M.; Soltan, A.; Anis, S. S. Facile approach for homogeneous dispersion of metallic silver nanoparticles on the surface of mesoporous titania for photocatalytic degradation of methylene blue and indigo carmine dyes. *J. Photochem. Photobiol., A* **2017**, *335*, 40−51.

(70) Gnaser, H.; Savina, M. R.; Calaway, W. F.; Tripa, C. E.; Veryovkin, I. V.; Pellin, M. J. Photocatalytic degradation of methylene blue on nanocrystalline TiO2: surface mass spectrometry of reaction intermediates. *Int. J. Mass Spectrom.* **2005**, *245* (1−3), 61−67.

(71) Tripathi, R.; Hameed, P.; Pragadeeshwara Rao, R.; Shrivastava, N.; Mittal, J.; Mohapatra, S. Biosynthesis of Highly Stable Fluorescent Selenium Nanoparticles and the Evaluation of Their Photocatalytic Degradation of Dye. *BioNanoScience* **2020**, *10*, 389 DOI: 10.1007/s12668-020-00718-0.

(72) Kshirsagar, A. S.; Gautam, A.; Khanna, P. K. Efficient photocatalytic oxidative degradation of organic dyes using CuInSe2/TiO2 hybrid hetero-nanostructures. *J. Photochem. Photobiol., A* **2017**, *349*, 73−90.

(73) Liu, C.; Lin, Y.; Dong, Y.; Wu, Y.; Bao, Y.; Yan, H.; Ma, J. Fabrication and investigation on Ag nanowires/TiO2 nanosheets/graphene hybrid nanocomposite and its water treatment performance. *Advanced Composites and Hybrid Materials* **2020**, *3* (3), 402−414.

(74) Barick, K. C.; Sharma, P.; Mukhija, A.; Sainis, J. K.; Gupta, A.; Hassan, P. A. Effect of cetylpyridinium chloride on surface passivation and photocatalytic activity of ZnO nanostructures. *Journal of Environmental Chemical Engineering* **2015**, *3* (2), 1346−1355.

(75) Wu, K.; Shi, M.; Pan, X.; Zhang, J.; Zhang, X.; Shen, T.; Tian, Y. Decolourization and biodegradation of methylene blue dye by a ligninolytic enzyme-producing Bacillus thuringiensis: Degradation products and pathway. *Enzyme Microb. Technol.* **2022**, *156*, No. 109999.

(76) Rashid, J.; Saleem, S.; Awan, S. U.; Iqbal, A.; Kumar, R.; Barakat, M.; Arshad, M.; Zaheer, M.; Rafique, M.; Awad, M. Stabilized fabrication of anatase-TiO 2/FeS 2 (pyrite) semiconductor composite nanocrystals for enhanced solar light-mediated photocatalytic

degradation of methylene blue. *RSC Adv.* **2018**, *8* (22), 11935−11945.

(77) Khnifira, M.; El Hamidi, S.; Mahsoune, A.; Sadiq, M.; Serdaroğlu, G.; Kaya, S.; Qourzal, S.; Barka, N.; Abdennouri, M. Adsorption of methylene blue cationic dye onto brookite and rutile phases of titanium dioxide: Quantum chemical and molecular dynamic simulation studies. *Inorg. Chem. Commun.* **2021**, *129*, No. 108659.

(78) Harisankar, A.; Preethi, P.; Mary, Y. S.; Sreeja, T.; Raghunandan, R. Spectral, thermal, structural and DFT studies of new luminescent heterobimetallic MOF of lead and sodium based on diglycolic acid ligand having unusual coordination environment for photodegradation and antibacterial applications. *J. Mol. Struct.* **2023**, *1285*, No. 135472.

(79) Nataraj, A.; Balachandran, V.; Karthick, T. Molecular orbital studies (hardness, chemical potential, electrophilicity, and first electron excitation), vibrational investigation and theoretical NBO analysis of 2-hydroxy-5-bromobenzaldehyde by density functional method. *J. Mol. Struct.* **2013**, *1031*, 221−233.

(80) Khnifiraa, M.; El Hamidia, S.; Machrouhia, A.; Mahsounea, A.; Boumyaa, W.; Tounsadia, H.; Mahjoubia, F. Z.; Sadiqa, M.; Barkaa, N.; Abdennouria, M. Theoretical and experimental study of the adsorption characteristics of Methylene Blue on titanium dioxide surface using DFT and Monte Carlo dynamic simulation. *Homo* **2020**, *190*, 393 DOI: 10.5004/dwt.2020.25737.

(81) Liu, Q.; Ren, P.; Wang, X.; Li, Y.; Yang, Y. Experimental and theoretical investigation of the photoelectrical properties of tetrabromophenol blue-and bromoxylenol blue-based solar cells. *J. Nanomater.* **2018**, *2018*, No. 9720595, DOI: 10.1155/2018/9720595.

(82) Contreras, M.; Grande-Tovar, C. D.; Vallejo, W.; Chaves-López, C. Bio-removal of methylene blue from aqueous solution by Galactomyces geotrichum KL20A. *Water* **2019**, *11* (2), 282.

(83) Shahzadi, T.; Zaib, M.; Riaz, T.; Shehzadi, S.; Abbasi, M. A.; Shahid, M. Synthesis of eco-friendly cobalt nanoparticles using Celosia argentea plant extract and their efficacy studies as antioxidant, antibacterial, hemolytic and catalytical agent. *Arabian Journal for Science and Engineering* **2019**, *44*, 6435−6444.

(84) Rubab, K.; Abbasi, M. A.; Siddiqui, S. Z.; Shah, S. A. A.; Ashraf, M.; Ahmad, I.; Lodhi, M. A.; Ghufran, M.; Shahid, M.; Fatima, H. Synthesis, pharmacological screening and computational analysis of some 2-(1H-Indol-3-yl)-N'-[(un) substituted phenylmethylidene] acetohydrazides and 2-(1H-Indol-3-yl)-N'-[(un) substituted benzo-yl/2-thienylcarbonyl] acetohydrazides. *Pak. J. Pharm. Sci.* **2017**, *30* (4), 1263−1275.

(85) Salehi, K.; Daraei, H.; Teymouri, P.; Maleki, A. Hydrothermal synthesis of surface-modified copper oxide-doped zinc oxide nanoparticles for degradation of acid black 1: Modeling and optimization by response surface methodology. *J. Adv. Environ. Health Res.* **2014**, *2* (2), 101−109.

(86) Dennington, R.; Keith, T. A.; Millam, J. M. *GaussView 6.0. 16*; Semichem Inc.: Shawnee Mission, KS, USA, 2016; pp 143−150.

(87) Sharma, D.; Singh, T. A DFT study of polyaniline/ZnO nanocomposite as a photocatalyst for the reduction of methylene blue dye. *J. Mol. Liq.* **2019**, *293*, No. 111528.

(88) Burke, K. Perspective on density functional theory. *J. Chem. Phys.* **2012**, *136* (15), 150901 DOI: 10.1063/1.4704546.

(89) Frisch, M. J.; Trucks, G. W.; Schlegel, H. B.; Scuseria, G. E.; Robb, M. A.; Cheeseman, J. R.; Scalmani, G.; Barone, V.; Mennucci, B.; Petersson, G. A. et al., *Gaussian09, R. A. 1*; gaussian. Inc.: Wallingford CT, 2009; Vol. *121*, pp 150−166.

(90) Al-Otaibi, J. S.; Mary, Y. S.; Mary, Y. S. DFT analysis of valproic acid adsorption onto Al12/B12-N12/P12 nanocages with solvent effects. *J. Mol. Model.* **2022**, *28* (4), 98.

(91) Alshabib, M.; Oluwadamilare, M. A.; Tanimu, A.; Abdulazeez, I.; Alhooshani, K.; Ganiyu, S. A. Experimental and DFT investigation of ceria-nanocomposite decorated AC derived from groundnut shell for efficient removal of methylene-blue from wastewater effluent. *Appl. Surf. Sci.* **2021**, *536*, No. 147749.

(92) Buvaneswari, M.; Santhakumari, R.; Usha, C.; Jayasree, R.; Sagadevan, S. Synthesis, growth, structural, spectroscopic, optical, thermal, DFT, HOMO−LUMO, MEP, NBO analysis and thermodynamic properties of vanillin isonicotinic hydrazide single crystal. *J. Mol. Struct.* **2021**, *1243*, No. 130856.